Available online at www.sciencedirect.com
ScienceDirect
International Journal of Heat and Fluid Flow 28 (2007) 1531–1544
International Journal of HEAT AND FLUID FLOW
www.elsevier.com/locate/ijhff

Three-dimensional numerical study and field synergy principle analysis of wavy fin heat exchangers with elliptic tubes

Y.B. Tao, Y.L. He *, Z.G. Wu, W.Q. Tao

State Key Laboratory of Multiphase Flow in Power Engineering, School of Energy & Power Engineering, Xi'an Jiaotong University, Xi'an, Shaan xi 710049, China

Received 4 August 2006; received in revised form 16 December 2006; accepted 15 February 2007
Available online 3 April 2007

Abstract

Three dimensional numerical studies were performed for laminar heat transfer and fluid flow characteristics of wavy fin heat exchangers with elliptic/circular tubes by body-fitted coordinates system. The simulation results of circular tube were compared with the experiment data, then circular and elliptic ($e = b/a = 0.6$) arrangements with the same minimum flow cross-sectional area were compared. A max relative heat transfer gain of up to 30% is observed in the elliptic arrangement, and corresponding friction factor only increased by about 10%. The effects of five factors on wavy fin and elliptic tube heat exchangers were examined: Reynolds number (based on the smaller ellipse axis, $500 \sim 4000$), eccentricity (b/a, $0.6 \sim 1.0$), fin pitch ($F_p/2b$, $0.05 \sim 0.4$), fin thickness ($F_t/2b$, $0.006 \sim 0.04$) and tube spanwise pitch ($S_1/2b$, $1.0 \sim 2.0$). The results show that with the increasing of Reynolds number and fin thickness, decreasing of the eccentricity and spanwise tube pitch, the heat transfer of the finned tube bank are enhanced with some penalty in pressure drop. There is an optimum fin pitch ($F_p/2b = 0.1$) for heat transfer, but friction factor always decreases with increase of fin pitch. And when $F_p/2b$ is larger than 0.25, it has little effects on heat transfer and pressure drop. The results were also analyzed from the view point of field synergy principle. It was found that the effects of the five factors on the heat transfer performance can be well described by the field synergy principle.

Keywords: Wavy fin; Elliptic tube heat exchanger; Field synergy principle; Numerical simulation

1. Introduction

Fin-and-tube heat exchangers are widely used in many engineering applications, for example, applications in such areas like air conditioning units, process gas heaters and coolers, compressor intercoolers, etc. Since majority of the thermal resistance of fin-and-tube heat exchanger is on the air side, improving air side fin and tube configurations, enhancing their heat transfer is the most effective way to improve the performance of the heat exchanger. There are two conventional methods for enhancing air side heat transfer, one is circular tube heat exchanger with wavy fin or slit fin and the other is elliptic tube with plain plate fin.

A lot of experimental and numerical studies have been conducted on airside heat transfer performances of wavy fin and circular tube heat exchangers. Wang et al. (1997, 1999) made extensive experiments on the heat transfer and pressure drop characteristics of wavy fin and tube heat exchangers. Jang and Chen (1997) numerically studied the heat transfer and fluid flow in a three-dimensional wavy fin-and-tube heat exchanger. Somchai and Yutasak (2005) experimentally investigated the effect of fin pitch and number of tube rows on the air side performance of herringbone wavy fin and tube heat exchangers. Manglik et al. (2005) analyzed the effects of fin density on low Reynolds number forced convection flow in three-dimensional wavy-plate-fin compact channels by numerical simulation.

* Corresponding author. Tel.: +86 29 82663851; fax: +86 29 82669106.
E-mail address: yalinghe@mail.xjtu.edu.cn (Y.L. He).

0142-727X/$ - see front matter © 2007 Elsevier Inc. All rights reserved.
doi:10.1016/j.ijheatfluidflow.2007.02.001

Nomenclature

a	larger ellipse semi-axis (m)
A	surface or cross-sectional area (m^2)
b	smaller ellipse semi-axis (m)
C_p	specific heat (J/kg K)
D	tube outside side diameter (m)
e	ellipse eccentricity, b/a
f	friction factor
F_p	fin pitch (m)
F_t	fin thickness (m)
h	heat transfer coefficient (W/m^2K)
k	thermal conductivity (W/m K)
L	flow length (m)
M	module production
N	the number of control volume or point
Nu	average Nusselt number, $(h \cdot 2b)/k$
p	pressure (Pa)
Δp	pressure drop in flow direction (Pa)
$\bar{p}$	bulk average pressure (Pa)
Q	heat transfer capacity (W)
Re	Reynolds number based on smaller ellipse axis ($U_c 2b/\upsilon$)
S_1	spanwise tube pitch (m)
S_2	longitudinal tube pitch (m)
T	temperature (K)
T_{in}	inlet temperature (K)
T_w	wall temperature (K)
$\overline{T}$	bulk average temperature (K)
u,v,w x,y,z	velocity components (m/s)
u_{in}	frontal velocity (m/s)
U_c	velocity at the minimum cross sectional area (m/s)
$\vec{U}$	velocity vector (m/s)
U,V,W	transformed velocity (m/s)
W_p	wave pitch (m)
x,y,z	Cartesian coordinates

Greek symbols

α	wavy angle (°)
μ	dynamic viscosity (Pa s)
υ	kinematic viscosity (m^2/s)
ρ	density (kg/m^3)
θ	the local intersection angle (°)

Subscripts

in	inlet parameters
m	mean or average value
ξ,η,ζ	body-fitted coordinates
out	outlet parameters
w	at wall conditions
Γ	boundary segment

The plain plate fin and elliptic tube heat exchanger were studied experimentally by Brauer (1964), Jang and Yang (1998), Saboya and Saboya (2001). These studies showed that elliptic tubes presented more heat transfer than the circular ones. Matos et al. (2001) performed a two-dimensional heat transfer analysis of non-finned circular and elliptic tubes heat exchangers. Numerical results showed a relative heat transfer gain of up to 13% in the optimal elliptical arrangement, as compared to the optimal circular arrangement. Matos et al. (2004) presented a three-dimensional numerical and experimental geometric optimization study to maximize the total heat transfer between a bundle of finned tubes in a given volume and external flow for staggered arrangements of circular and elliptic tubes with plain plat fin. A relative heat transfer gain of up to 19% was observed in the optimal elliptic arrangement as compared to the optimal circular one.

The foregoing literature review shows that both wavy fin and elliptic tube can enhance heat transfer. All these published studies only reported the results with some explanations from convective heat transfer and fluid flow considerations, not enough in explaining why things happens the way it happened. In this study, the focus will be not only on the effects of the parameters on heat transfer and fluid flow but also on the physics of the reasons for enhancement or deterioration of the convective heat transfer with different parameter combinations. In 1998, Guo et al. (1998) proposed a novel concept about the enhancement of convective heat transfer for parabolic flow and showed that the reduction of the intersection angle between the velocity and temperature gradient can effectively enhance the heat transfer. Later, Tao et al. (2002a,b) demonstrated that this idea is also valid for elliptic flow if the flow Peclet number is not too small. This concept is now called as field synergy principle, since the word "synergy" means cooperative action of two forces or the like (Guralnik, 1979). An extension of the field synergy principle to more general transport phenomena was made by He (2002) and He et al. (2004), and a comprehensive review on the recent development of the study on the field synergy principle was conducted by Tao and He (2002), He and Tao (2002).

In this paper, the numerical study of a new type of fin-and-tube heat exchanger with wavy fin and elliptic tube was performed. The comparisons of the elliptic tube and circular tube arrangements were presented. The effects of five factors on the heat transfer and fluid flow of the new type heat exchanger were examined: Reynolds number, eccentricity, fin pitch, fin thickness and spanwise tube pitch. The results were explained from the view point of field synergy principle. Numerical simulation for wavy fin and elliptic tube heat transfer surface is conducted with

body-fitted coordinates system, and the volume average intersection angle between the velocity and temperature gradient and the module production of velocity and temperature gradient within the computational domain are determined. Then compare the trend of heat transfer with the trends of the average intersection angle and module production with the same parameters to see if the trends are consistent with the new concept. Numerical results show that the trends are consistent with the new concept very well.

The details of the field synergy principle can be found from the above-referenced papers, and for the simplicity of presentation, it is not re-stated here.

2. Model description

2.1. Physical model

The schematic diagram of a wavy fin and tube heat exchanger is shown in Fig. 1(a). Fig. 1(b) and (c) give a top view of the computation domain of the two-row wavy fin heat exchanger with circular and elliptic tube respectively, where the smaller ellipse axis of the elliptic tube equals to the outside diameter of the circular tube. The geometric parameters for the circular tube case are listed as following: the tube outside diameter (D) of 10.55 mm, fin pitch F_p as 2.096 mm, fin thickness (F_t) of 0.2 mm, spanwise tube pitch ($S1$) of 25.0 mm, longitudinal tube pitch ($S2$) of 21.65 mm, wave angle (α) at 17.44° and wave pitch (W_p) of 10.825 mm. The actual computation domain was 7.5 times of the original heat transfer zone. The domain was extended 1.5 times of the original heat transfer zone for the entrance section to ensure the inlet uniformity, and at the exit of heat transfer region, the domain was extended 5 times of the original heat transfer zone in order to make sure that the local one-way method can be used for the numerical treatment of the outer flow boundary condition. In Fig. 2, the pictorial view of the computational domain is presented, where the upstream and downstream parts of the computation domain are not presented proportionately in order to save the space. In these two parts of the computational domain a much coarser grid distribution was adopted to save the computing resource.

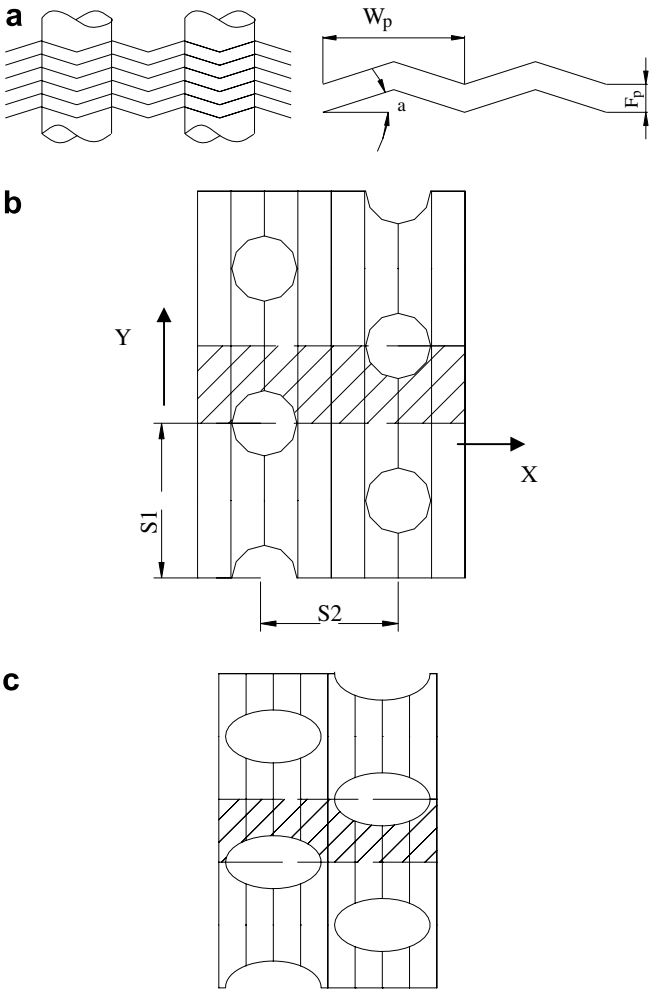

Fig. 1. Schematic diagram of a wavy fin-and-tube heat exchanger and computation domain. (a) Schematic of wavy fin-and-tube heat exchanger (b) Schematic of computational domain for circular tube (c) Schematic of computational domain for elliptic tube.

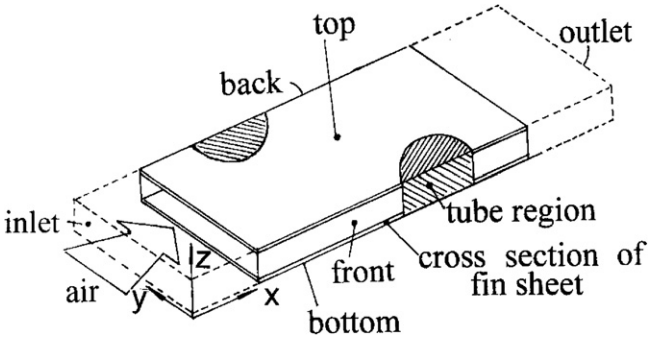

Fig. 2. A pictorial view of the computational domain.

2.2. Grid generation technique

Traditional methods to simulate the fin-and-tube heat exchanger were mostly performed in Cartesian coordinates, the step-approaching method was adopted at the tube surface, and this approximation method will cause some errors related to the grid precision. The more coarse of the grid, the larger of the error. Too fine grid will lead to more computation time, and the complicated computation domain makes the use of step-approaching method more difficult. In this paper, the body-fitted coordinates was adopted, it helps to transform the complex computational domain in real space into a simple domain in the transformed space.

The basic idea of the body-fitted coordinate is to numerically generate a curvilinear coordinate system having coordinate lines coincident with each boundary of the real computational domain, regardless of the shapes of these

boundaries. This is implemented by solving elliptic partial differential equations. Constant values of one of the curvilinear coordinates are specified as Dirichlet boundary conditions on each boundary. Values of the other coordinates are either specified by a monotonic variation over a boundary as Dirichlet boundary conditions, or determined by Neumann boundary conditions. In the latter case, the curvilinear coordinate lines can be made to intersect the boundary according to some specified conditions, such as being normal or parallel to some given directions. It is also possible to exercise control over the spacing of the curvilinear coordinate lines in the field in order to concentrate lines in regions of expected high gradients. In any case, the numerical generation of the coordinate system is done automatically for any shape boundaries, requiring only the input of points on the boundary.

In order to obtain a grid in the transformed space, a grid system generating method needs to be developed. The simplest equation that could be used to generate the grid is the Laplace's equations:

$$\nabla^2 \xi_i = 0, \quad i = 1, 2, 3 \tag{1}$$

The commonly used grid generation techniques are based on the Poisson equation proposed in Thompson et al. (1974). The 3D Poisson equation in the physical space can be expressed as:

$$\begin{aligned}
&\frac{\partial^2 \xi}{\partial^2 x} + \frac{\partial^2 \xi}{\partial^2 y} + \frac{\partial^2 \xi}{\partial^2 z} = P(\xi, \eta, \varsigma) \\
&\frac{\partial^2 \eta}{\partial^2 x} + \frac{\partial^2 \eta}{\partial^2 y} + \frac{\partial^2 \eta}{\partial^2 z} = Q(\xi, \eta, \varsigma) \\
&\frac{\partial^2 \varsigma}{\partial^2 x} + \frac{\partial^2 \varsigma}{\partial^2 y} + \frac{\partial^2 \varsigma}{\partial^2 z} = R(\xi, \eta, \varsigma)
\end{aligned} \tag{2}$$

where: P,Q,R are functions for controlling the spacing between coordinate lines. The above partial differential equations are subject to a set of Dirichlet boundary conditions, such as

$$\begin{bmatrix} \xi \\ \eta \\ \zeta \end{bmatrix} = \begin{bmatrix} \xi_1(x, y, z) \\ \eta_1 \\ \zeta_1(x, y, z) \end{bmatrix}, (x, y, z) \in \Gamma \tag{3}$$

where: η_1 is a specified constant, $\xi_1(x,y,z)$ and $\zeta_1(x,y,z)$ are specified monotonic functions on a boundary segment Γ.

The above equations are transformed into the computational space where the Cartesian coordinates are the dependent variables. Then we have:

$$\begin{aligned}
&\alpha_{11} x_{\xi\xi} + \alpha_{22} x_{\eta\eta} + \alpha_{33} x_{\zeta\zeta} + 2\alpha_{12} x_{\xi\eta} + 2\alpha_{13} x_{\xi\zeta} + 2\alpha_{23} x_{\eta\zeta} \\
&\quad + J^2 (P x_\xi + Q x_\eta + R x_\zeta) = 0 \\
&\alpha_{11} y_{\xi\xi} + \alpha_{22} y_{\eta\eta} + \alpha_{33} y_{\zeta\zeta} + 2\alpha_{12} y_{\xi\eta} + 2\alpha_{13} y_{\xi\zeta} + 2\alpha_{23} y_{\eta\zeta} \\
&\quad + J^2 (P y_\xi + Q y_\eta + R y_\zeta) = 0 \\
&\alpha_{11} z_{\xi\xi} + \alpha_{22} z_{\eta\eta} + \alpha_{33} z_{\zeta\zeta} + 2\alpha_{12} z_{\xi\eta} + 2\alpha_{13} z_{\xi\zeta} + 2\alpha_{23} z_{\eta\zeta} \\
&\quad + J^2 (P z_\xi + Q z_\eta + R z_\zeta) = 0
\end{aligned} \tag{4}$$

where: $\alpha_{jk} = \sum_{m=1}^{3} \beta_{mk} \beta_{mk}$, and β_{mk} is the cofactor of the (m,k) element in the matrix M:

$$M = \begin{bmatrix} x_\xi & x_\eta & x_\zeta \\ y_\xi & y_\eta & y_\zeta \\ z_\xi & z_\eta & z_\zeta \end{bmatrix}, \text{and } J = \det |M| \tag{5}$$

Thus,

$$\begin{aligned}
\alpha_{11} &= \beta_{11}^2 + \beta_{21}^2 + \beta_{31}^2 \\
\alpha_{22} &= \beta_{12}^2 + \beta_{22}^2 + \beta_{32}^2 \\
\alpha_{13} &= \beta_{13}^2 + \beta_{23}^2 + \beta_{33}^2 \\
\alpha_{12} &= \beta_{11}\beta_{12} + \beta_{21}\beta_{22} + \beta_{31}\beta_{32} \\
\alpha_{13} &= \beta_{11}\beta_{13} + \beta_{21}\beta_{23} + \beta_{31}\beta_{33} \\
\alpha_{23} &= \beta_{12}\beta_{13} + \beta_{22}\beta_{23} + \beta_{32}\beta_{33}
\end{aligned} \tag{6}$$

The transformed boundary conditions are:

$$\begin{bmatrix} x \\ y \\ z \end{bmatrix} = \begin{bmatrix} f_1(\xi, \eta_1, \zeta) \\ f_2(\xi, \eta_1, \zeta) \\ f_3(\xi, \eta_1, \zeta) \end{bmatrix}, (\xi, \eta_1, \zeta) \in \Gamma^* \tag{7}$$

where: $f_1(\xi,\eta_1,\zeta)$, $f_2(\xi,\eta_1,\zeta)$ and $f_3(\xi,\eta_1,\zeta)$ are determined by the known shape of the boundary segment Γ and the specified distribution of ξ thereon. Γ^* is the boundary segment of Γ in the transformed space.

In order to improve the quality of the generated grid system, especially for the parts of wave crest and wave trough, the final grid systems were generated by the block structured method with body-fitted coordinates (Tao, 2001). The pictures of the generated grid systems for the fin part will be presented in Section 3.

2.3. Governing equations

The governing equations in Cartesian coordinates are:

$$\text{Continuity equation} : \frac{\partial}{\partial x_i}(\rho u_i) = 0 \tag{8}$$

$$\text{Momentum equation} : \frac{\partial}{\partial x_i}(\rho u_i u_k) = \frac{\partial}{\partial x_i}\left(\mu \frac{\partial u_k}{\partial x_i}\right) - \frac{\partial p}{\partial x_k} \tag{9}$$

$$\text{Energy equation} : \frac{\partial}{\partial x_i}(\rho u_i T) = \frac{\partial}{\partial x_i}\left(\frac{k}{C_p}\frac{\partial T}{\partial x_i}\right) \tag{10}$$

The governing equations in the computational space are:

$$\frac{\partial}{\partial \xi}(\rho U) + \frac{\partial}{\partial \eta}(\rho V) + \frac{\partial}{\partial \varsigma}(\rho W) = 0 \tag{11}$$

$$\begin{aligned}
&\frac{\partial}{\partial \xi}(\rho U \Phi) + \frac{\partial}{\partial \eta}(\rho V \Phi) + \frac{\partial}{\partial \varsigma}(\rho W \Phi) = \frac{\partial}{\partial \xi}\left(\frac{\alpha}{J}\Gamma^\Phi \frac{\partial \Phi}{\partial \xi}\right) \\
&+ \frac{\partial}{\partial \eta}\left(\frac{\beta}{J}\Gamma^\Phi \frac{\partial \Phi}{\partial \eta}\right) + \frac{\partial}{\partial \varsigma}\left(\frac{\gamma}{J}\Gamma^\Phi \frac{\partial \Phi}{\partial \varsigma}\right) + JS
\end{aligned} \tag{12}$$

where: U,V and W are velocity components in transformed space.

$$U=\alpha_1u+\alpha_2v+\alpha_3w,\quad V=\beta_1u+\beta_2v+\beta_3w,\quad W=\gamma_1u+\gamma_2v+\gamma_3w,$$
$$J=x_\xi y_\eta z_\zeta+x_\eta y_\zeta z_\xi+x_\zeta y_\xi z_\eta-x_\zeta y_\eta z_\xi-x_\eta y_\xi z_\zeta-x_\xi y_\zeta z_\eta \tag{13}$$

2.4. Boundary conditions

The fluid is assumed to be incompressible with constant property and the flow is laminar and in steady state condition. The fin surfaces are considered as part of the solution domain and will be treated as a special type of fluid with infinite viscosity, but with actual thermal conductivity. The heat conduction in the fins is considered. In the fins, the periodic conditions are adopted to solve energy equation, and the temperatures in the fins are determined by the full-field computation method. The governing equations are discretized by using the control volume method (Tao, 2001). The SIMPLE algorithm is used to ensure the coupling between velocity and pressure. The convection term is discretized by the power-law scheme.

The boundary conditions are described for the three regions as follows.

(a) In the upstream extended region

At the inlet boundary:

$$u=u_{\text{in}}=\text{const},\quad v=w=0,\quad T=T_{\text{in}}=\text{const}$$

At the upper and lower boundaries:

$$\frac{\partial u}{\partial z}=\frac{\partial v}{\partial z}=0,\quad w=0,\quad \frac{\partial T}{\partial z}=0$$

At the front and back boundaries:

$$\frac{\partial u}{\partial y}=\frac{\partial w}{\partial y}=0,\quad v=0,\quad \frac{\partial T}{\partial y}=0$$

(b) In the downstream extended region

At the upper and lower boundaries:

$$\frac{\partial u}{\partial z}=\frac{\partial v}{\partial z}=0,\quad w=0,\quad \frac{\partial T}{\partial z}=0$$

At the front and back boundaries:

$$\frac{\partial u}{\partial y}=\frac{\partial w}{\partial y}=0,\quad v=0,\quad \frac{\partial T}{\partial y}=0$$

At the outlet boundary:

$$\frac{\partial u}{\partial x}=\frac{\partial v}{\partial x}=\frac{\partial w}{\partial x}=\frac{\partial T}{\partial x}=0$$

(c) In the fin coil region

At the upper and lower boundaries:

Velocity condition: $u=v=w=0$

Temperature condition: periodic conditions

At the front and back boundaries:

$$\text{Fluid region}:\frac{\partial u}{\partial y}=\frac{\partial w}{\partial y}=0,\quad v=0,\quad \frac{\partial T}{\partial y}=0$$

$$\text{Fin surface region}:u=v=w=0,\quad \frac{\partial T}{\partial y}=0$$

$$\text{Tube region}:u=v=w=0,\quad T=T_w=\text{const}$$

3. Parameter definitions and grid independency validation

The definitions of Re, average Nu number and friction factor are as follows.

$$Re=U_cD/\upsilon, Nu=hD/k, f=\Delta pD/[(1/2)\rho U_c^2L] \tag{14}$$

where: U_c, υ, and λ are the air velocity in the minimum flow cross-section of the tube row, kinetic viscosity and thermal conductivity, D is the outside diameter for circular tube and the smaller ellipse axis for elliptic tube, Δp is the pressure drop along the air flow direction, and L is the fin length along the air flow direction.

The mean temperature and pressure of a cross-section are defined as:

$$\overline{T}=\frac{\int\int_A uTdA}{\int\int_A udA},\quad \overline{p}=\frac{\int\int_A pdA}{\int\int_A dA} \tag{15}$$

The total heat transfer, pressure drop and log-mean temperature difference are expressed as:

$$Q=\dot{m}C_p(\overline{T}_{\text{out}}-\overline{T}_{\text{in}}),\quad \Delta P=\bar{p}_{\text{in}}-\bar{p}_{\text{out}},$$
$$\Delta T=\frac{(T_w-\overline{T}_{\text{in}})-(T_w-\overline{T}_{\text{out}})}{\ln[(T_w-\overline{T}_{\text{in}})/(T_w-\overline{T}_{\text{out}})]}. \tag{16}$$

The heat transfer coefficient is defined as: $h=Q/(A\Delta T)$, where A is the total air side heat transfer area (both tube and fin surface).

For the presentation of numerical results in terms of the field synergy principle, the following parameter is introduced:

$$M=\sum|\vec{U}||gradT|/N \tag{17}$$

where: N is the total number of the control volume. Obviously, the value of M corresponds to the full synergy case, where the intersection angle between velocity and temperature gradient becomes zero, and the production of velocity vector and temperature gradient is the largest. For simplicity it will be called module production.

The local intersection angle is determined by the following equation

$$\theta=\cos^{-1}\frac{u\frac{\partial T}{\partial x}+v\frac{\partial T}{\partial y}+w\frac{\partial T}{\partial z}}{|\vec{U}||gradT|} \tag{18}$$

And from the local intersection angle, the average intersection angle of the computation domain of the fin area can be obtained by using numerical integration,

$$\theta_m=\frac{\sum\theta_{i,j,k}dv_{i,j,k}}{\sum dv_{i,j,k}} \tag{19}$$

where: $dv_{i,j,k}$ is the volume element of the control volume (i, j, k).

In order to validate the solution independency of the grid number, four different grid systems are investigated. They are $78\times12\times12$, $142\times12\times12$,$142\times22\times12$, $142\times32\times12$. The predicted averaged Nu numbers for the four grid system are shown in Fig. 3. From the figure it can be seen that the solution of the grid system of

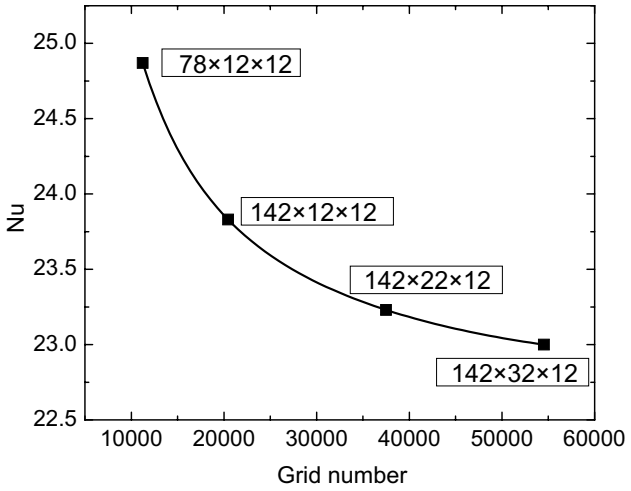

Fig. 3. Variation of the predicted Nusselt number with grid number systems at $Re = 1000$.

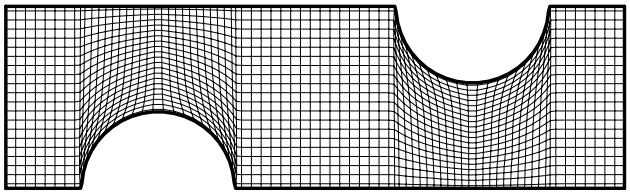

Fig. 4. Grid system generated by body-fitted coordinates.

$142 \times 22 \times 12$ can be regarded as grid-independent. In order to check the grid system in z-direction, the grid system $142 \times 22 \times 22$ was studied and found that at $Re = 1000$, the grid $142 \times 22 \times 22$ yields a Nu number about 2% lower than that of the grid $142 \times 22 \times 12$. So the system $142 \times 22 \times 12$ is adopted in the following calculations. Similar examinations were also conducted for the other cases. The grid systems generated by body-fitted coordinates are illustrated in Fig. 4. Only the fin region is presented in the figure for simplicity.

4. Simulation results and discussions

The effects of the Reynolds number, eccentricity, fin pitch, fin thickness and spanwise tube pitch on heat transfer and fluid flow were analyzed by the self-developed code. The simulation results were discussed and analyzed from the view point of field synergy principle. The major results are presented in the following section.

4.1. Code validation, Re number effect and the comparisons of elliptic and circular tube arrangements

In order to validate the reliability of the numerical simulation procedure and the self-developed code, numerical simulation was carried out at the same fin and tube geometrical configurations as presented in Xin et al. (1994). Schematic and geometric parameters of the fin and tube heat exchanger are shown in the physical model (see Section 2.1). The Re number defined in Eq. (14) ranges from 500 to 4000, the corresponding frontal air velocity ranges from 0.464 to 3.71 m/s. The results of the simulations and the comparisons between simulation and experiment are shown in Fig. 5(a) and (b), where the experimental correlations of the Nu and f are adopted from Xin et al. (1994). As can be seen from the figures, the agreements are very good, with the mean deviation in Nu and f being 3.3 and 1.9 percent, respectively.

Then the comparisons of the heat transfer and fluid flow characteristics of circular tube and elliptic tube ($e = b/a = 0.6$) arrangements with the same minimum flow cross-sectional area (the smaller ellipse axis equals to the outside diameter of the circular tube) were performed. It can be seen from Fig. 5(a) that with the increase of Reynolds number, the Nu number of both circular tube and elliptic tube increase, and the values of elliptic tube are always larger than that of circular tube. Within the range of the calculation, the Nu number of elliptic tube can be enhanced up to 30% due to the tube surface and air flow velocity in fin coil of the elliptic tube larger than those of circular tube. At the same time the friction factor of both elliptic tube and circular tube decrease with the increase of Reynolds number, and the friction factors of the elliptic tube are always larger than circular tube because the flow velocity of the elliptic tube arrangement is higher than the circular one. The max friction factor increase is about 10%. This result implies that the elliptic tube arrangement can greatly enhance the heat transfer with a little penalty in pressure drop when compared to circular tube arrangement.

There may be has a question. As all of us known, the elliptic tube is more accordant to air dynamics and the pressure drop of elliptic tube should be smaller than circular one. Why is the friction factor of the elliptic tube larger than circular one? In order to study the problem, the simulations are performed for the elliptic tube (elliptic tube B) with the same tube perimeter as circular tube and the smaller friction factors in elliptic tube B case are found as shown in Fig. 5(c). The elliptic tube A is the one studied in above paragraphs, which has the same minimum flow cross-section area with circular tube case. The widths of the computational domain for the three cases are same. The difference between the two elliptic tubes is that the air flow cross-section area of the elliptic tube A is smaller than that of the elliptic tube B, as shown in Fig. 5(d). The total air flow rates are same for the three cases, so the flow velocity in the fin coil of the elliptic tube A is higher than the circular tube and the elliptic tube B, which leads to the pressured drop of the elliptic tube A is larger than circular tube and elliptic tube B. In Fig. 5(c) the friction factor is defined based on the inlet velocity and fin pitch, in other sections, the friction factor is defined as Eq. (14).

Fig. 6(a) shows the variation of the average intersection angle between velocity and temperature gradient and

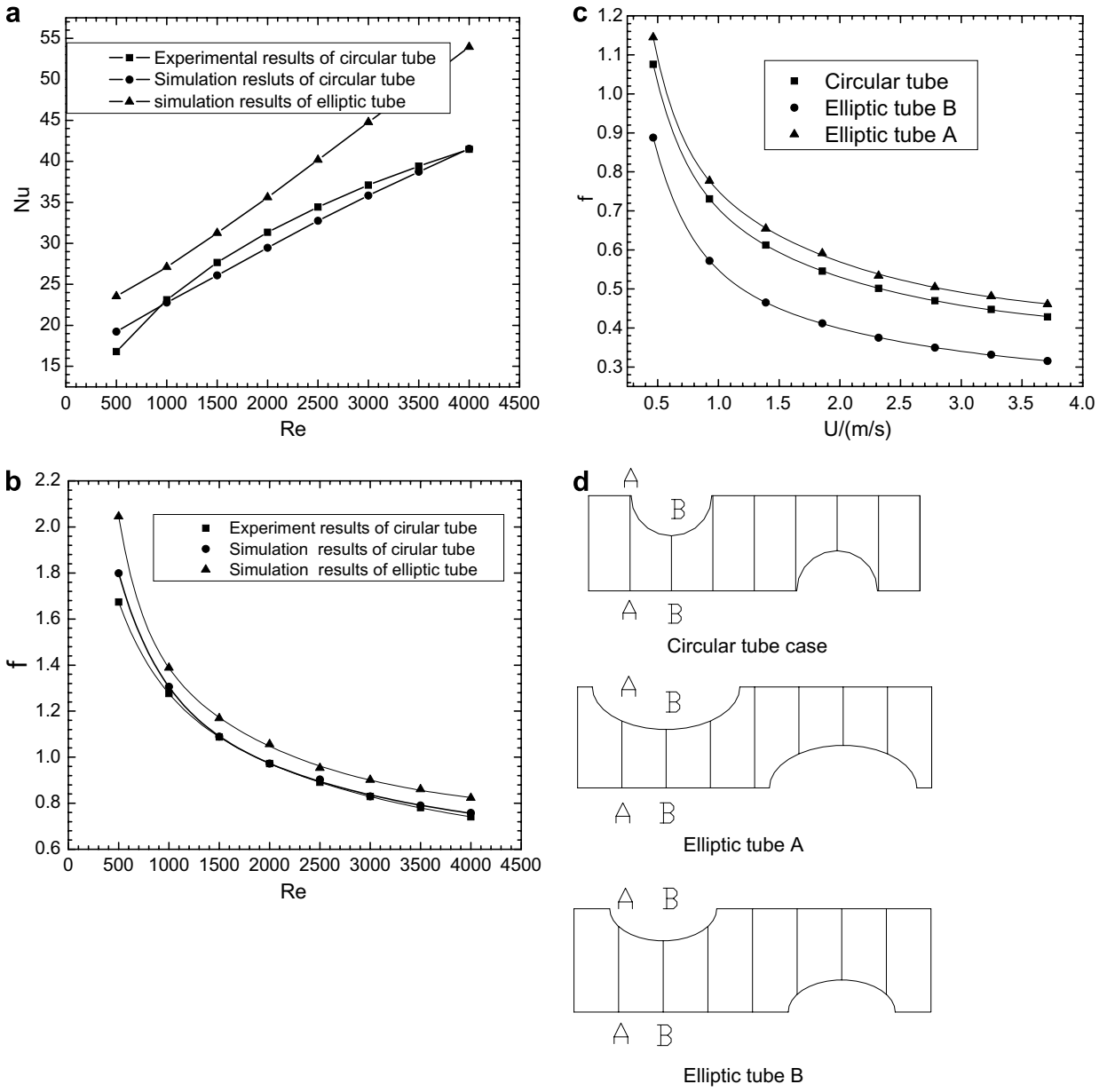

Fig. 5. Effects of *Re* on *Nu* and *f*. (a) Effect of *Re* on *Nu*; (b) effect of *Re* on *f*; (c) effect of *Re* on *f* of different tube cases; (d) schematic of the flow cross-section of the three cases.

Fig. 6(b) provides the relation of $M \sim Re$ for both circular tube and elliptic tube. It can be seen from Fig. 6(a) that the average intersection angle increases with increasing *Re* number, which implies the deterioration of the synergy between velocity and temperature gradient. The intersection angle of elliptic tube is larger than that of circular tube, which indicates the synergy effect of the elliptic tube is worse than circular tube. But Fig. 6(b) shows that the value of *M* is quickly increased with the increase of *Re* number. The value of elliptic tube is larger than that of the circular tube and the increasing degree of module production is larger than intersection angle. The positive effect resulted from the module production increase is much larger than the negative effect of the intersection angle increase. Thus it becomes clear that the increase of average *Nu* number with replacing circular tube by elliptic tube is resulted from the increase in module production, and which is accordant with field synergy principle.

The local flow and thermal fields at different Reynolds are presents in Fig. 6(c), (d) and (e). With the increasing of the Reynolds number, the streamlines in most parts are the same, but the circumfluence region at the back of the tube increase. More and more isothermals incline to the streamline with increasing Re number, especially at the back half region, which increases the intersection angle between velocity and temperature gradients as shown in Fig. 6(a). The increase of the circumfluence region also decreases the synergy effect.

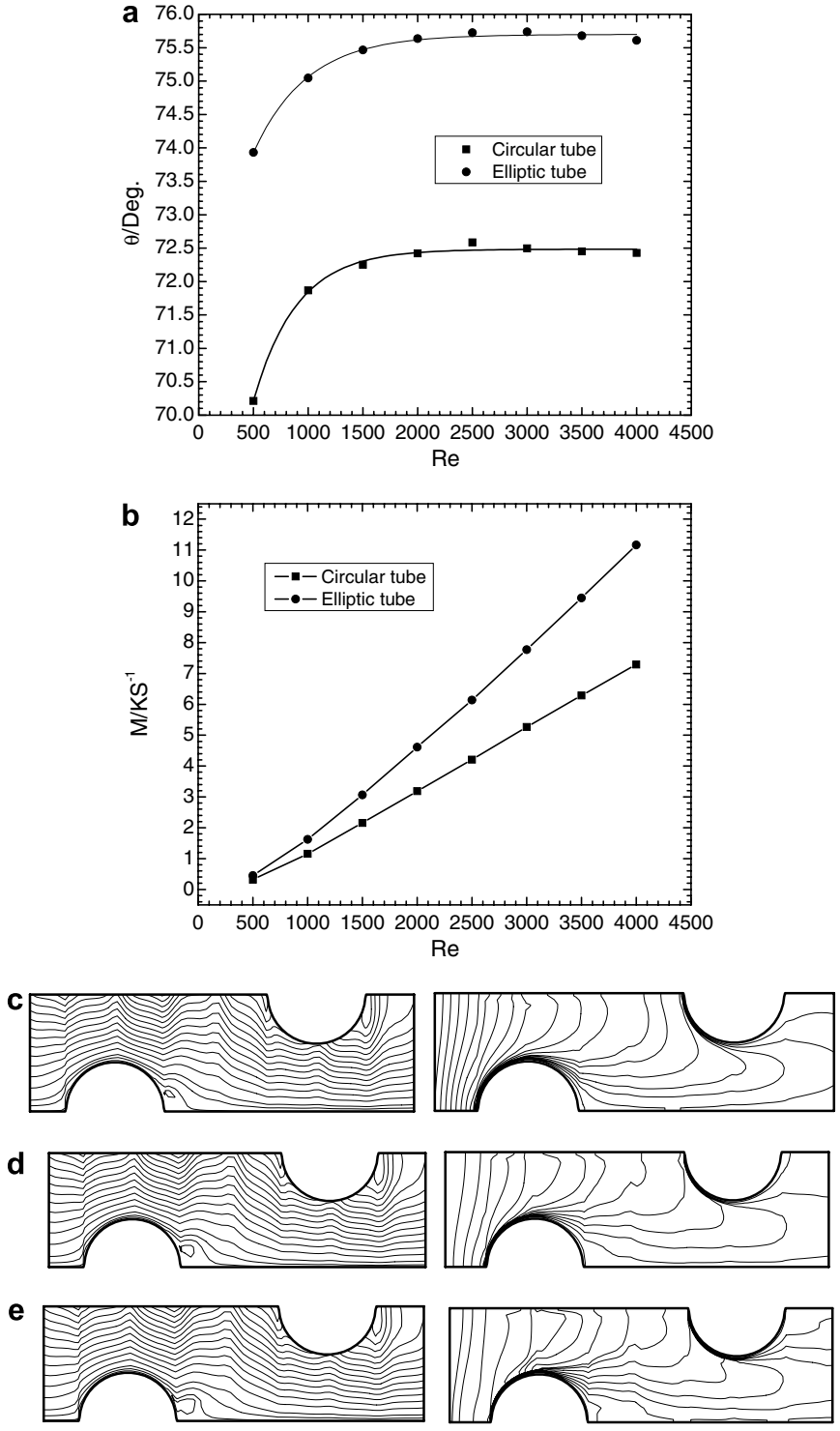

Fig. 6. Variations of intersection angle and module production with *Re*. (a) Variation of intersection angle; (b) variation of module production; (c) streamlines and isothermals of the middle section in z-direction at $Re = 500$; (d) streamlines and isothermals of the middle section in z-direction at $Re = 1000$; (e) streamlines and isothermals of the middle section in z-direction at $Re = 2000$.

4.2. Eccentricity effect

For examining the effects of the eccentricity on heat transfer and fluid flow, the simulations were performed under the same parameter conditions as circular tube defined in physical model, only the eccentricity of the elliptic tube was changed from 0.6 to 1.0, and the smaller ellipse axis always equals to the outside diameter of the circular tube. The Reynolds number is taken as 1000 (the corresponding inlet velocity is 0.927 m/s).

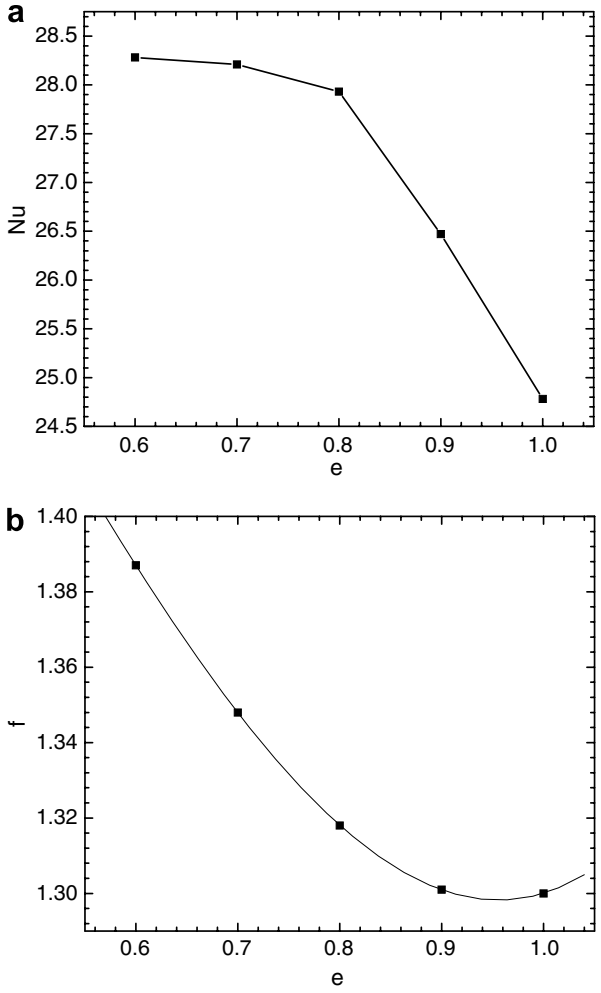

Fig. 7. Variations of average *Nu* and *f* with eccentricity. (a) Variation of average *Nu* with eccentricity; (b) variation of average *f* with eccentricity.

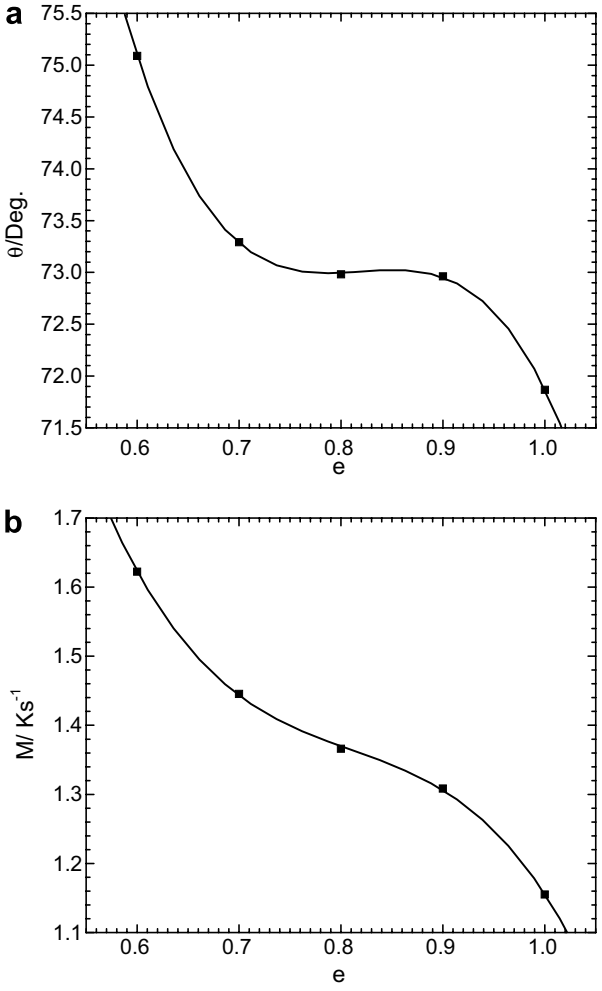

Fig. 8. Variations of average intersection angle and module production with eccentricity. (a) Variation of intersection angle; (b) variation of module production.

Fig. 7(a) shows the relation of *Nu* number and eccentricity. It can be seen that the *Nu* number decreases with the increase of eccentricity. The decreasing tendency is slower at first, and then it decreases quickly with the increase of eccentricity. Because of limited by the geometry parameter of the physical model, the eccentricity varies only from 0.6 to 1.0, and in this range the optimal eccentricity is not been observed. But analyzing from the tendency, we can infer that there exists an optimal eccentricity. In Fig. 7(b), the effect of eccentricity on friction factor is presented, where the friction factor decreases quickly with the increase of the eccentricity at first, and then it slows down, and at last it almost keeps as constant which is almost contrary to the variety tendency of *Nu* number. With the increase of the elliptic eccentricity, the elliptic tube more and more approaches to circular tube, so the heat transfer and pressure drop more and more near to circular tube. The relations between *Nu*, friction factor and eccentricity are accordant with the conclusions in Section 4.1.

The field synergy presentations are provided in Fig. 8. It can be concluded from Fig. 8(a) that with the increase of the eccentricity the average intersection angle decreases quickly at eccentricity less than 0.7, then it slows down at $0.7 \sim 0.9$, and decreases quickly again at eccentricity larger than 0.9. The variety tendency of the module production is similar to the intersection angle, but the degree is more tempered. And from further comparison between the effects of intersection angle decrease and the module production decrease, it can be found that the negative effect resulted from the module production decrease is much larger than the positive effect of the intersection angle decrease. The decrease of average *Nu* with the increase of eccentricity is resulted from the decrease of the module production.

4.3. Fin pitch effect

The effects of the fin pitch on average Nusselt number and friction factor are shown in Fig. 9. The non-dimensional fin pitch based on smaller ellipse axis varies from 0.05 to 0.4, eccentricity equals to 0.6 and the other parameters (F_t,S_1,S_2,α and W_p) remain the same as circular tube

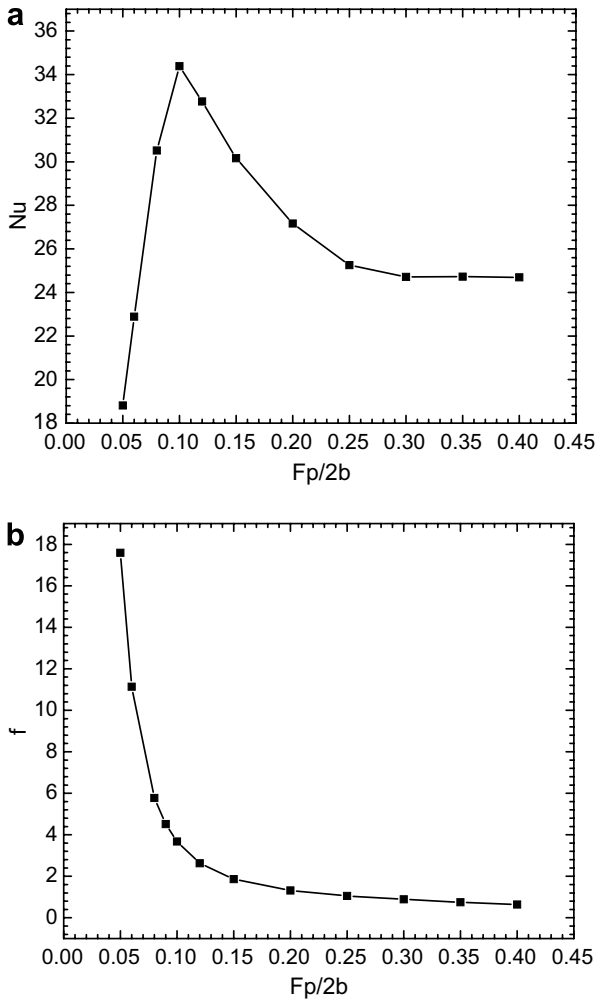

Fig. 9. Variations of average *Nu* and *f* with fin pitch. (a) Variation of average *Nu* with fin pitch; (b) variation of average *f* with fin pitch.

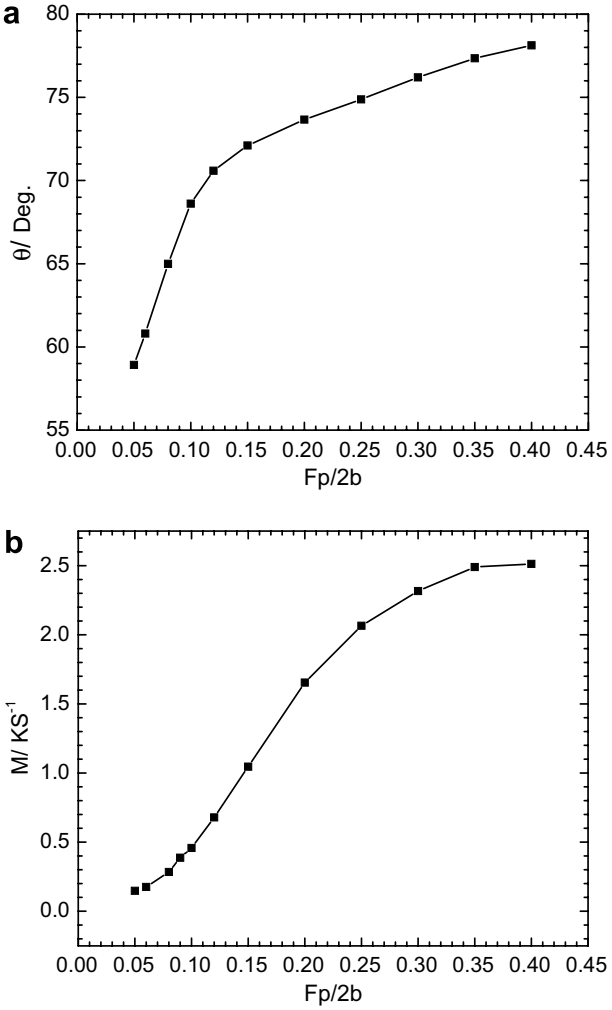

Fig. 10. Variations of average intersection angle and module production with fin pitch. (a) Variation of intersection angle; (b) variation of module production.

defined in physical model. The Reynolds number is taken as 1000 (the corresponding inlet velocity is 0.927 m/s).

Fig. 9(a) shows the relation of fin pitch and *Nu* number. It can be seen that the *Nu* number reaches the maximum at the non-dimensional fin pitch $F_p/2b$ of 0.1. Departure away from this fin pitch will lead to the decrease of the average *Nu* number. When the non-dimensional fin pitch is larger than 0.25, the fin pitch has little effect on the average *Nu* number. The effect of fin pitch on the friction factor is presented in Fig. 9(b), which indicates that with the increase of the fin pitch, *f* will always decrease, and when the non-dimensional fin pitch is larger than 0.25, the fin pitch has little effect on *f* too.

The field synergy presentations are provided in Fig. 10. It can be concluded from the results that the increase of fin pitch leads to the increase in the intersection angle, which is very sensitive to the fin pitch at first, and once the non-dimensional fin pitch is greater than 0.25, the dependence becomes weaker with increasing fin pitch. The module production increase with the increase of fin pitch too, and after the fin pitch reaches 0.25, the dependency is weaker and weaker, which is accordant with the variety tendency of *Nu*. The intersection angle increases with the increase of the fin pitch, at the same time the module production increase too. So there exists an optimal fin pitch at which the Nu is the maximum. This is coincident with the tendency of the Nu vs. fin pitch, as shown in Fig. 9(a). And the optimum *Nu* number presents to the fin pitch, at which the module production increases most strongly. So, we can say the effect of the fin pitch on *Nu* number is coincident with the field synergy principle.

4.4. Fin thickness effect

For examining the fin thickness effect, the simulation were performed for differential non-dimensional fin thickness varied from 0.006 to 0.04, the eccentricity equals to 0.6 with smaller ellipse axis equaling to circular tube outside diameter, the other parameters (F_p,S_1,S_2,α and W_p) are the same as circular tube defined in physical model. And the Reynolds number is taken as 1000 (the corresponding inlet

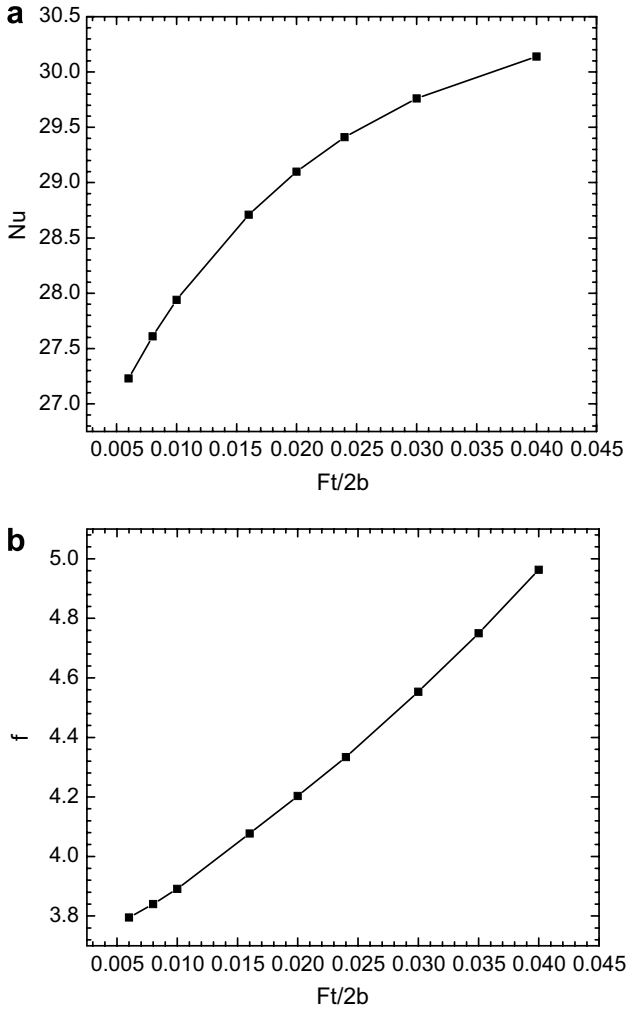

Fig. 11. Variations of average *Nu* and *f* with fin thickness. (a) Variation of average *Nu* with fin thickness; (b) variation of average *f* with fin thickness.

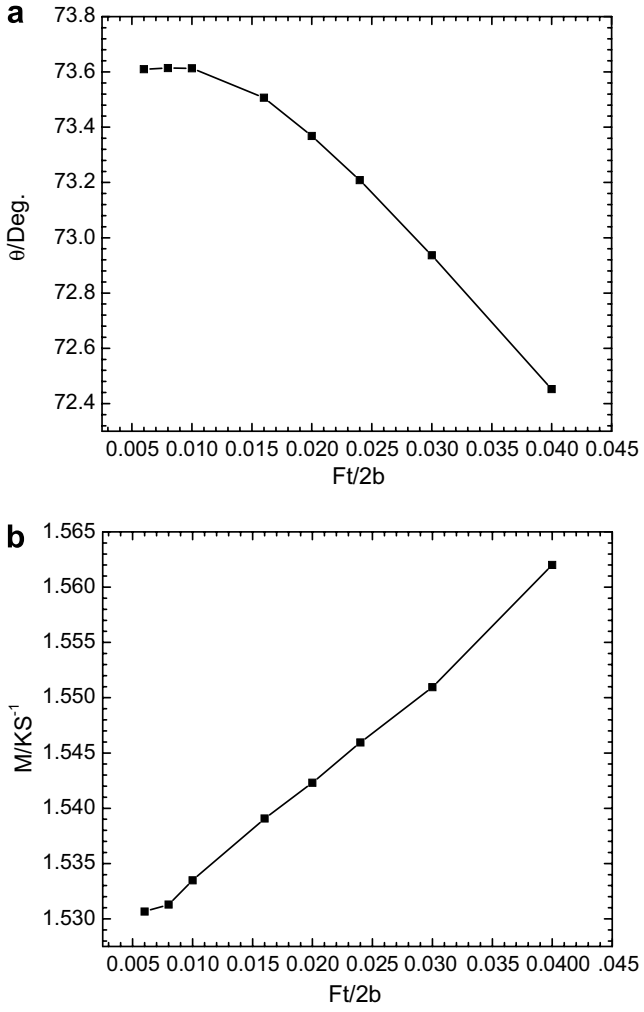

Fig. 12. Variations of average intersection angle and module production with fin thickness. (a) Variation of intersection angle; (b) variation of module production.

velocity is 0.927 m/s). The results are shown in Fig. 11. Because the minimum free flow cross-sectional area decreases with the increase of fin thickness, which leads to the increase of the velocity in the minimum flow cross-section, so in this section, the Reynolds number and friction factor are both based on the inlet velocity in stead of the velocity at the minimum flow cross-section.

Fig. 11(a) shows the variation of the average *Nu* number with the non-dimensional fin thickness. According to the figure, the *Nu* number increases with the increase of fin thickness, but the increasing tendency is weakened gradually. The effects of the thermal resistance in the fins increase with the increase of the fin thickness, which leads to the decrease of the heat transfer capacity. The increase of the *Nu* number is due to the increase of the velocity in the fin coil. The friction factor based on total pressure drop increases with the increase of fin thickness, and the increasing tendency is strengthened gradually due to the increase of the air flow velocity in the fin coil and entrance contraction and exit expansion.

The intersection angle is provided in Fig. 12(a). The average angle decreases with the increase of fin thickness, and the decrease tendency is very little at non-dimensional fin thickness less than 0.01, then the decrease tendency increase gradually. But the module production increase with the fin thickness increase. With the increase of fin pitch, the average intersection angle decrease and module production increase, so the increase of fin thickness leading to the increase of average *Nu* number is accordant with field synergy principle.

4.5. Spanwise tube pitch effect

The effects of spanwise tube pitch on heat transfer and fluid flow are presented in Fig. 13. The non-dimensional spanwise tube pitch based on smaller ellipse axis varies from 1.0 to 2.0, eccentricity equals to 0.6 with smaller ellipse axis equaling to circular tube outside diameter and the inlet velocity is taken as 0.927 m/s. Because the mini-

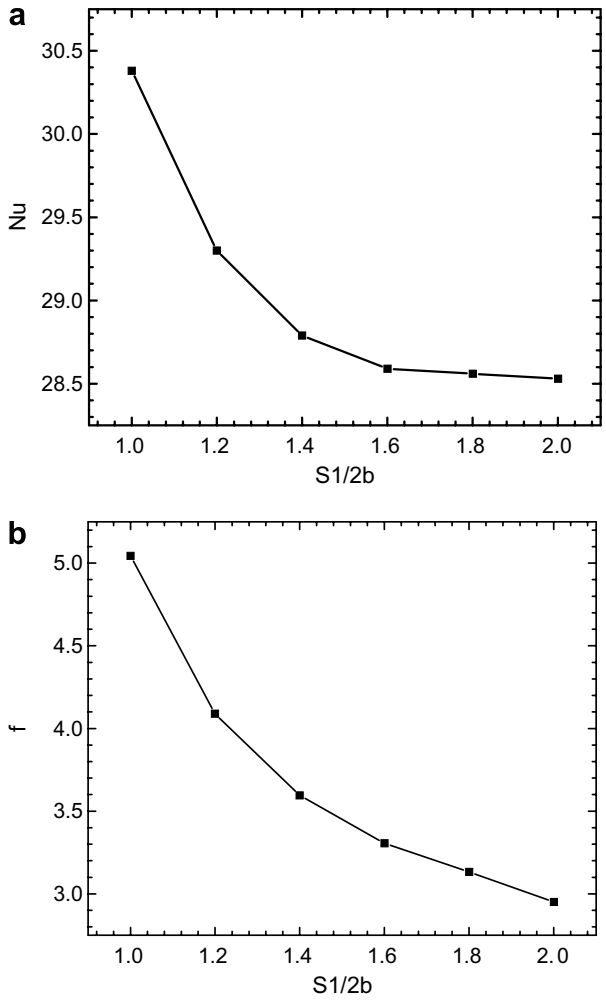

Fig. 13. Variations of average *Nu* and *f* with spanwise tube pitch. (a) Variation of average *Nu* with spanwise tube pitch; (b) variation of average *f* with spanwise tube pitch.

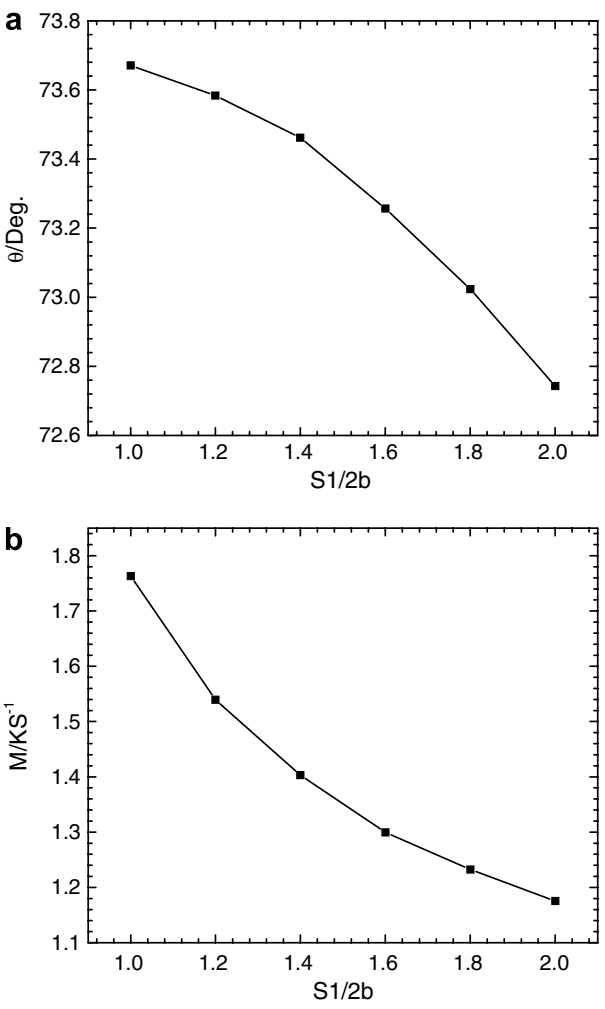

Fig. 14. Variations of average intersection angle and module production with spanwise tube pitch. (a) Variation of intersection angle; (b) variation of module production.

mum free flow cross-sectional area increases with the increase of spanwise tube pitch, which leads to the decrease of the velocity in the minimum flow cross-section, so in this section, the Reynolds number and friction factor are both based on the inlet velocity, and in other sections the definitions are expressed in Eq. (14).

The average *Nu* number decreases with the increase of the spanwise tube pitch and the decrease tendency slows down gradually, after the non-dimensional spanwise tube pitch reaches 1.6, the increase of tube pitch has little effect on average *Nu* number, as shown in Fig. 13(a). Fig. 13(b) presents the relation of friction factor and spanwise tube pitch, the friction factor decreases with the increase of the tube pitch and the tendency is weaker and weaker. With the increase of the spanwise tube pitch, the velocity in the fin coil decreases, so the heat transfer and pressure drop both decrease.

The relation of intersection angle and spanwise tube pitch is shown in Fig. 14(a). The average intersection angle decreases with the increase of the spanwise tube pitch. And the module production is shown in Fig. 14(b). It can be seen that with the increase of the spanwise tube pitch the module production decreases too. And further comparison between the effects of intersection angle decrease and the module production decrease, it can be found that the negative effect resulted from the module production decrease is much larger than the positive effect of the intersection angle decrease. Thus it can be concluded that the decrease of average *Nu* with the increase of spanwise tube pitch is resulted from the decrease of module production, which is coincident with the field synergy principle.

5. Conclusions

In this paper, 3-D numerical simulations are conducted to compare the heat transfer and fluid flow characteristics between wavy fin heat exchangers with circular tube and elliptic tube arrangements, and the effects of the Reynolds number, eccentricity, fin pitch, fin thickness and spanwise

tube pitch on the heat transfer and fluid flow characteristics of wavy fin and elliptic tube heat transfer surfaces were examined. The numerical results are analyzed from the view point of the field synergy principle. The effects of the five factors on the heat transfer performance can be well described by the field synergy principle. The following conclusions can be made.

(1) For wavy fin and tube heat exchangers, the elliptic tube arrangement can enhance heat transfer by 30% and friction factor increases only about 10%, when compared to circular tube arrangement with the same flow obstruction cross-sectional area. So, the wavy fin and elliptic tube can greatly enhance heat transfer with a little penalty in pressure drop and will be widely used in the field of enhancement heat transfer.
(2) The increase of *Re* number leads to the increase of the *Nu* number and the decrease of *f*. The synergy effect of velocity and temperature gradient becomes worse and worse with *Re* number increase. The enhancement of heat transfer is due to the increase of the module production of velocity and temperature gradient.
(3) The average *Nu* number and friction factor decrease with the increase of the eccentricity. The decreasing tendency of *Nu* number is slow at first, and then it decreases suddenly with the increase of eccentricity when eccentricity is larger than 0.8. The friction factor decreases quickly at first, and then the decrease tendency slows down at eccentricity larger than 0.8. The decrease of the *Nu* number is resulted from the decrease of the module production.
(4) There is an optimum fin pitch ($F_p/2b = 0.1$) at which the *Nu* number is the maximum, and the corresponding variety tendency of module production is the most strong. But *f* always decreases with the increase of fin pitch. And when $F_p/2b$ is larger than 0.25, it has little effects on heat transfer and pressure drop.
(5) Both *Nu* number and *f* increase with the increase of fin thickness due to the increase of the air flow velocity in the fin coil. The increase of average *Nu* number can also be explained from the decrease in the intersection angle between the velocity and temperature gradient and the increase of the module production.
(6) The average *Nu* number and *f* factor decrease with the increase of spanwise tube pitch. The decrease tendency of *Nu* number slows down gradually, after the non-dimensional spanwise tube pitch reaches 1.6, the increase of tube pitch has little effect on average *Nu* number. The friction factor decreases generally with tube pitch and the tendency is weaker and weaker. The decrease of the *Nu* number is due to the decrease of the module production.
(7) Some more studies such as the effects of the parameters on fin efficiency could be done in the following research.

Acknowledgement

The present work is supported by the National Science Fund for Distinguished Young Scholars from the National Natural Science Foundation of China (No. 50425620), National Basic Research Program of China (973 Program)(2007CB206902) and the Key Grant Project of Chinese Ministry of Education (NO.306014).

References

Brauer, H., 1964. Compact heat exchangers. Chem. Process Eng. (August), 451–460.

Guo, Z.Y., Li, D.Y., Wang, B.X., 1998. A novel concept for convective heat transfer enhancement. International Journal of Heat and Mass Transfer 41, 2221–2225.

Guralnik, D.B., Editor-in-chief, 1979. WEBSTER'S New Word Dictionary of the American Language. 2nd college edition. William Collins Publishers, Inc., Cleveland, 1444.

He, Y.L., 2002. Theoretical and experimental investigations on the performance improvements of split-stirling cryocooler and pulse tube refrigerator. Ph.D. Thesis, Xi'an Jiaotong University.

He, Y.L., Tao, W.Q., 2002. Field synergy principle and its application in enhancing convective heat transfer and improving performance of pulse tube refrigerator, Part II. J. Xi'an Jiaotong Univ. 36, 1106–1110.

He, Y.L., Wu, M., Tao, W.Q., Chen, Z.Q., 2004. Improvement of the thermal performance of pulse tube refrigerator by using a general principle for enhancing energy transport and conversion processes. J. Appl. Therm. Energy 24, 79–93.

Jang, J.Y., Chen, L.K., 1997. Numerical analysis of heat transfer and fluid flow in a three-dimensional wavy-fin and tube heat exchanger. International Journal of Heat and Mass Transfer 40 (16), 3981–3990.

Jang, J.Y., Yang, J.Y., 1998. Experimental and 3-D numerical analysis of the thermal hydraulic characteristics of elliptic finned-tube heat exchangers. Heat Transfer Eng. 19 (4), 55–67.

Manglik, R.M., Zhang, J.H., Muley, A., 2005. Low Reynolds number forced convection in three-dimensional wavy-plate-fin compact channels: fin density effects. International Journal of Heat and Mass Transfer 48, 1439–1449.

Matos, R.S., Vargas, J.V.C., Laursen, T.A., Saboya, F.E.M., 2001. Optimization study and heat transfer comparison of staggered circular and elliptic tubes in forced convection. Internal Journal of Heat and Mass Transfer 44, 3953–3961.

Matos, R.S., Laursen, T.A., Vargas, J.V.C., Bejan, A., 2004. Three-dimensional optimization of staggered finned circular and elliptic tubes in forced convection. International Journal of Thermal Sciences 43, 477–487.

Saboya, S.M., Saboya, F.E.M., 2001. Experiments on elliptic sections in one and two-row arrangements of plate fin and tube heat exchangers. Exp. Therm. Fluid Sci. 24, 67–75.

Somchai, W., Yutasak, C., 2005. Effect of fin pitch and number of tube rows on the air side performance of herringbone wavy fin and tube heat exchangers. Energy Conversion & Management 46, 2216–2231.

Tao, W.Q., 2001. Heat Transfer, second ed. Xi'an Jiaotong University Press, Xi'an.

Tao, W.Q., He, Y.L., 2002. Field synergy principle and its application in enhancing convective heat transfer and improving performance of pulse tube refrigerator, Part I. J. Xi'an Jiaotong Univ. 36, 1101–1105.

Tao, W.Q., Guo, Z.Y., Wang, B.X., 2002a. Field synergy principle for enhancing convective heat transfer-its extension and numerical verifications. International Journal of Heat and Mass Transfer 45, 3849–3856.

Tao, W.Q., He, Y.L., Wang, Q.W., Qu, Z.G., Song, F.Q., 2002b. A unified analysis on enhancing single phase convective heat transfer

with field synergy principle. International Journal of Heat and Mass Transfer 45 (24), 4871–4879.

Thompson, J.F., Thames, F.C., Mastin, C.W., 1974. Automatic numerical generation of body-fitted curvilinear coordinate system for field containing any number of arbitrary two-dimensional bodies. J. Compt. Physics 15, 299–319.

Wang, C.C., Fu, W.L., Chang, C.T., 1997. Heat transfer and friction characteristics of typical wavy fin-and-tube heat exchangers. Heat Transfer and Friction Characteristics 14, 174–186.

Wang, C.C., Jang, J.Y., Chiou, N.F., 1999. A heat transfer and friction correlation for wavy fin-and-tube heat exchangers. International Journal of Heat and Mass Transfer 42, 1919–1924.

Xin, R.C., Li, H.Z., Kang, H.J., Li, W., Tao, W.Q., 1994. An experimental investigation on heat transfer and pressure drop characteristics of triangular wavy fin-and-tube heat exchanger surfaces. J. Xi'an Jiaotong Univ. 28 (2), 77–83.